Journal of New Technology and Materials (JNTM)
J. New Technol. Mater.
Vol. 12, N°02 (2022)54-61

OEB Univ. Publish. Co.

Concept and realization of a specimen grips A and B for tensile tests adapted to specimens cut transversely from the tube

I. Mouallif [a]*, O. Zhouri [a], I. Haddouch [a], A. Benrhzyal [b], Z. Mouallif [c], B. Radi [c], A. Hachim [d], A. Ghollam and M. Chergui [e]

[a] *L2MC, ENSAM, Université Moulay Ismail (UMI), BP 15290, Al Mansour, Meknès, Morocco.*

[b] *FS, Faculté des Sciences, Université Ibn Tofail, BP 133, Kenitra, Morocco.*

[c] *LIMII, FST, Université Hassan 1er, BP 577, Route de Casa, Settat, Morocco.*

[d] *Laboratory of Materials and Structures, Institute of Maritime Studies, BP 20100, Casablanca, Morocco.*

[e] *LCCMMS, ENSEM, Université Hassan II (UH2C), BP 8118, Casablanca, Morocco*

*Corresponding author, email: i.mouallif@ensam.umi.ac.ma

Received date: Aug. 17, 2022 ; revised date: Nov. 2, 2022; accepted date: Nov. 4, 2022

Abstract

Composite pipes must comply to avoid the risks of degradation (mechanical, and physico-chemical). To verify the mechanical resistance of these pipes, we prepared standardized specimens in longitudinal, transverse directions and CT and DCB types. In order to perform tensile tests on the MTS 810 tensile (or fatigue) machine, flat specimens are widely used, but transversely cut specimens and CT and DCB types are not widely used. The main objective of this scientific paper is the innovation of two steel grips A and B, which will allow to fix specimens inside the jaws of tensile (or fatigue) machines in order to obtain reproducible tests. This docking and alignment device transform the non-limiting tensile (or fatigue) machine, with the rapid adaptation of the tensile machine jaws capable of clamping specimens of complex geometric shapes.

Keywords: Composites; Tensile test; fatigue machine; Docking and alignment; steel grips; Mechanical realization;

1. Introduction

The sewerage system is designed to evacuate the liquid waste, which ensures protection against sanitary diseases and flooding risks. The pipes are made of different materials, namely: Reinforced concrete [6], PVC (polyvinyl chloride)[11], GRP (glass fiber reinforced polyester) [7], HDPE (high density polyethylene) .... These pipes must meet quality standards to ensure sustainable use. The composite is a heterogeneous and anisotropic material, to test it mechanically it is necessary to investigate the mechanical properties in both directions of the pipes [1-2]. We may point to some literature evaluation that examined the mechanical behavior of polymer samples under tensile effects.

Hong Zhang conducted a study of the effect of specimen geometry on the performance of tensile tests by individually changing the specimen width and gauge length. They showed that the compliance of the system is only related to the specimen width, but is not sensitive to the gauge length and polymer film thickness. [12]
Sary A.Malak proposed models to predict the stress-strain relationship including modulus of elasticity, toughness, stress and strain in proportional, ultimate and failure states of a recyclable polyvinyl chloride/calcium carbonate (PVC/CaCO3) thermoformable composite mineral board. The developed models are essential to establish the requirements and design criteria for structural elements equipped with this type of composite. [13]

These tests will be carried out on a uni-axial servo-hydraulic machine, connected to a data acquisition chain allowing the recording of the displacement and the load as a function of time. The information will be stored and processed by a computer using the TESTWORKS software [3].

Tensile tests are performed on specimens in the form of flat, transverse samples (Figure 1), or CT and DCB sections in cylindrical tubes.

The flat specimens are easily attached to the original jaws of the MTS 810 machine (Figure 3), but the other specimens (cross-sections, DCB and CT) cannot be attached (due to their 20 mm width exceeding the jaw opening) [4].

The objective of this work is the creation of two devices (A: for cross-cut specimens, and B: for CT and DCB specimens) to perform tensile and fatigue tests on specimens of different types. These two specimen grippers form the mechanical link between the specimen and the testing machine.

Then a numerical simulation was performed, using the finite element method with ANSYS software, in order to know the performance of these devices.[G],[H]
For future work, experimental testing of these grips is recommended to ensure that the specimens are fixed in the jaws of the tensile machine, Several research groups have applied this approach to polymer materials [16],[17],[18],[19]

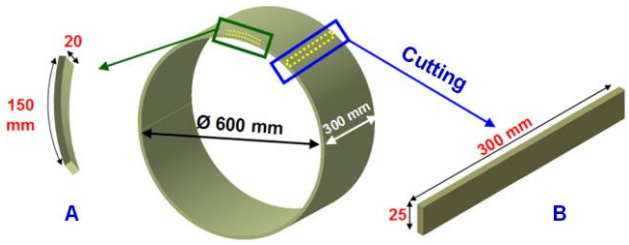

Figure 1. Types of standardized specimens which are cut according to two directions of the pipelines (A: Longitudinal, B: Transverse) [9]

2. Method

2.1. Design of the device

The mooring and alignment devices A and B are composed of five parts (a, b, c, d, e) (figure 4 corresponding to device A) (figure 6 corresponding to device B), their dimensions and geometries are given by the computer aided design software (CATIA V5) [5].

2.2. Material

The material chosen for the manufacture of the device is ordinary steel XC 10. The tables below show its mechanical properties and chemical composition.

Table1: Mechanical properties of the material

Diameter	**R**	**Re**	**A**	**KCU à +20°C**
mm	MPa	MPa	%	J/cm²
40 < d ≤ 100	320-420	≥ 205	≥ 29	≥ 100

Table2: Chemical composition of the material

C	**Si**	**Mn**	**P**	**S**
0.07-0.13	≤ 0,40	0.30-0.60	≤ 0,035	≤ 0,035

2.3. Fabrication

The making of devices is carried out within the workshop of mechanical manufacture by various machines with tools of machining (Numerical control milling machine, Turning, Drilling, Manual surface grinding machine). These are presented in the following figure (figure 2).

Figure 2. Different steps of realization

After machining, the assembly of these device parts is carried out in order to adapt to different types of specimens with complex geometrical shapes (figure 5).

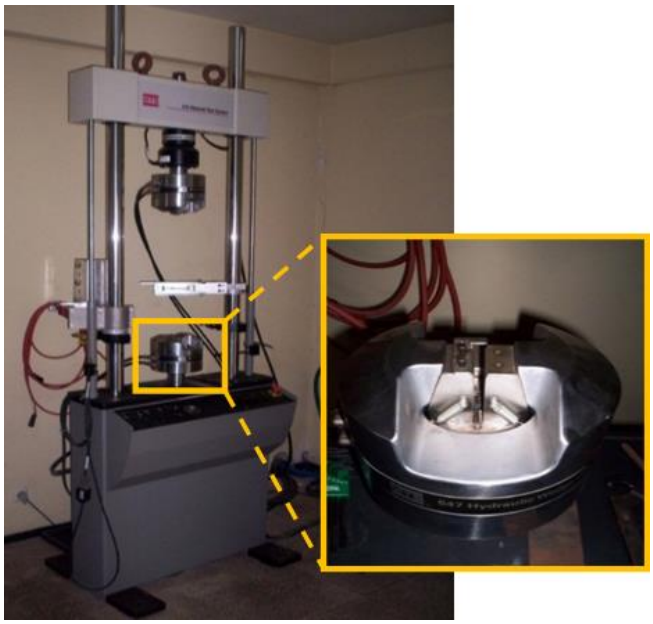

Figure 3. Jaws of the MTS 810 machine

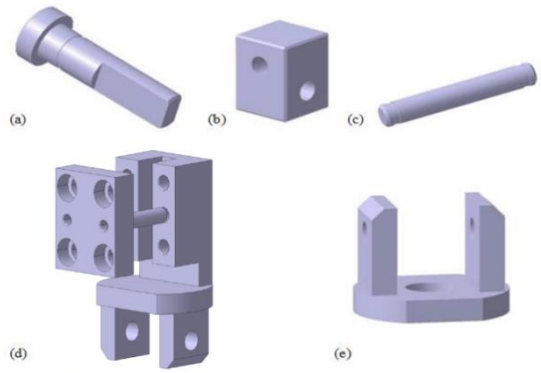

Figure 4. Different parts of the device A that are drawn with CATIA V5 software

Figure 5. Realized device A (grips)

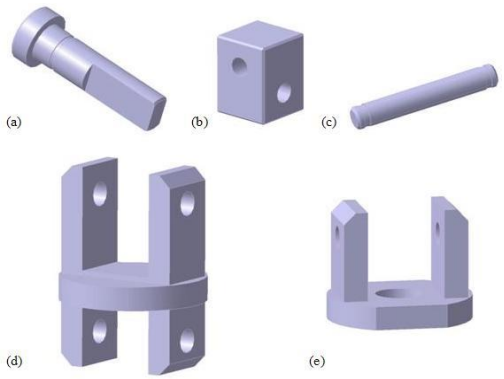

Figure 6. Different parts of the device B that are drawn with CATIA V5 software.

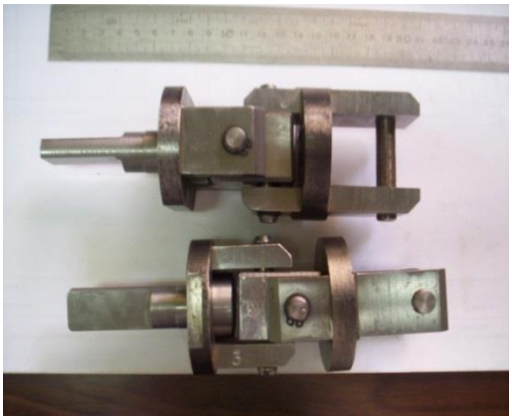

Figure 7. Realized device B (grips).

3. Results and discussions

We carried out a numerical simulation, using the finite elements method by the software ANSYS, on the devices in order to identify: the total deformation, the equivalent elastic stress and the equivalent stress of Von Mises [6-7, 10].

3.1. Mesh and boundary conditions

In order to have precise results of the analysis, we used a mesh by volume elements of type SOLID 185 and of order 1mm, (figures 8 and 9).

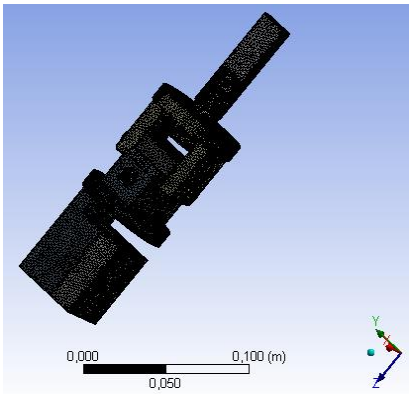

Figure8. Mesh of the studied structure by volumetric elements of type SOLID 185 (ANSYS) of the device A

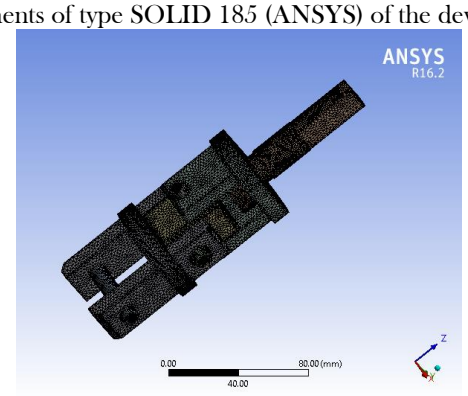

Figure 9. Mesh of the studied structure by volumetric elements of type SOLID 185 (ANSYS) of the device B.

Regarding the modeling of forces on device A, they were made by an embedded link at point B, and a tensile force applied at point A. For the modeling of the forces on device B, they were made by a link embedded at point A, and a tensile force applied at point B.

We used four different forces: F_1 = 2000N, F_2 = 3000N, F_3 = 4000N, F_4 = 5000 N, in order to study the behavior of both devices A and B.

Through the simulation of our devices, we sought to highlight the stress field developed from the loads applied (Force F) on devices A and B, these simulations are performed using ANSYS software.

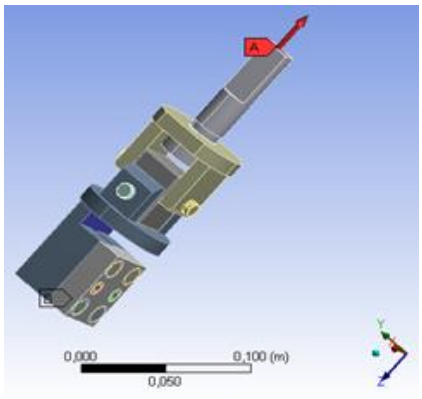

Figure 10. Geometric modeling and assembly boundary conditions of the device A.

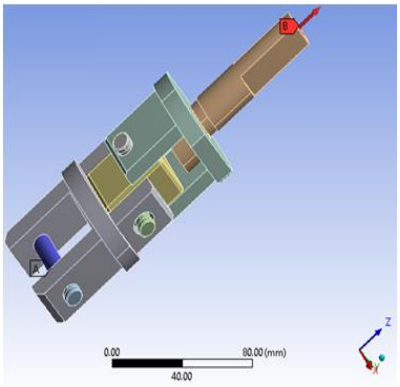

Figure 11. Geometric modeling and assembly boundary conditions of the device B.

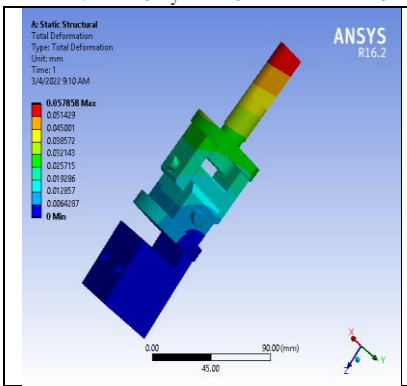

Figure 12. Total deformation for device A (F_1=2000N)

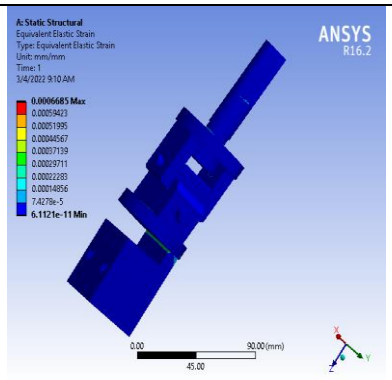

Figure 14. Equivalent elastic strain for device A (F_1=2000N)

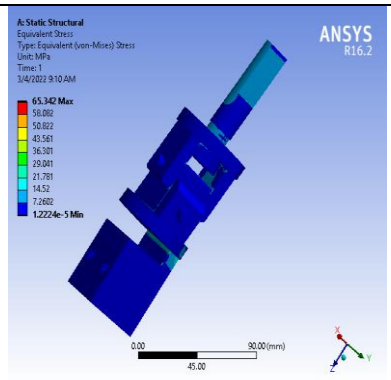

Figure 16. Equivalent (von-Mises) Stress for device A (F_1=2000N)

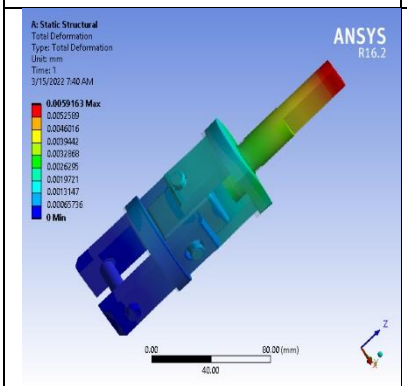

Figure 13. Total deformation for device B (F1=2000N)

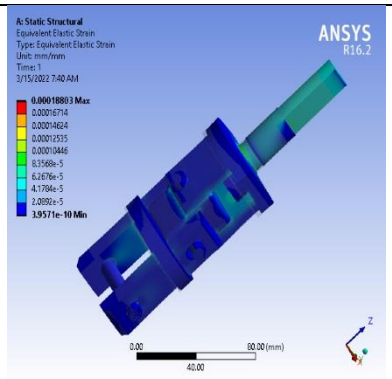

Figure 15. Equivalent elastic strain for device B (F1=2000N)

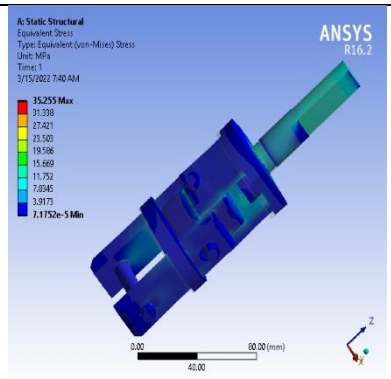

Figure 17. Equivalent (von-Mises) Stress for device B (F1=2000N)

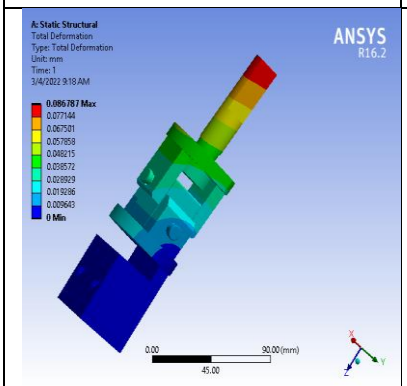

Figure 18. Total deformation for device A (F2=3000N)

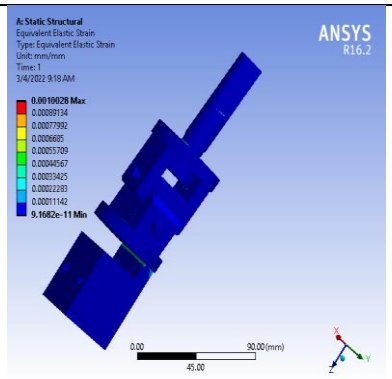

Figure 20. Equivalent elastic strain for device A (F2=3000N)

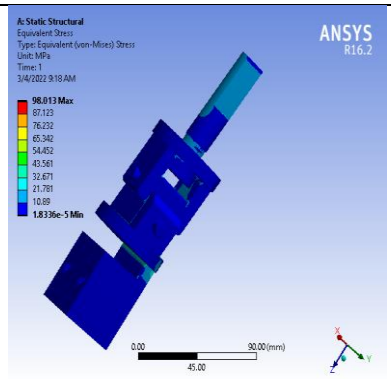

Figure 22. Equivalent (von-Mises) Stress for device A (F2=3000N)

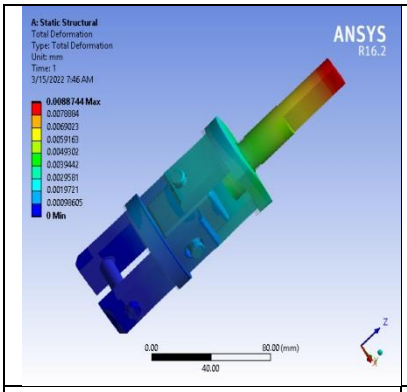	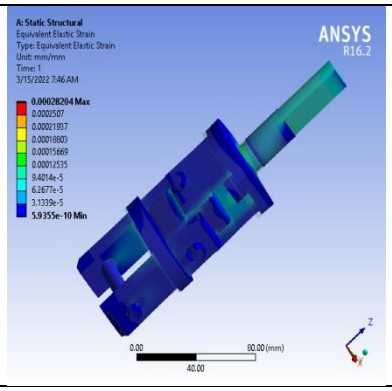	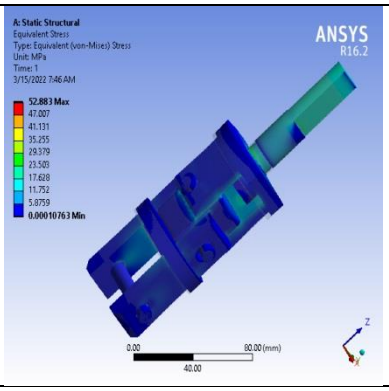
Figure 19. Total deformation for device B (F2=3000N)	Figure 21. Equivalent elastic strain for device B (F2=3000N)	Figure 23. Equivalent (von-Mises) Stress for device B (F2=3000N)
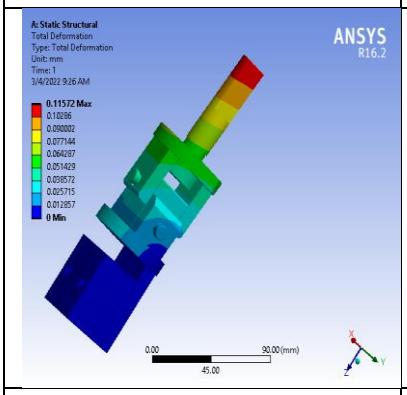	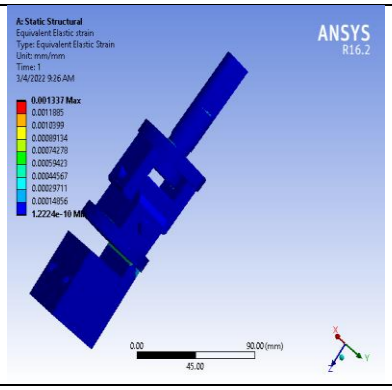	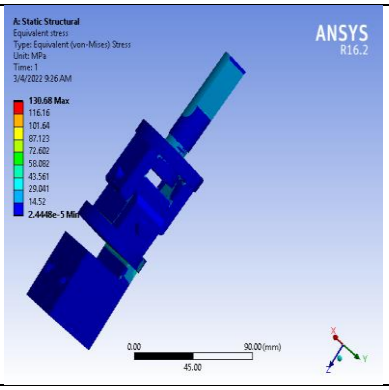
Figure 24. Total deformation for device A (F3=4000N)	Figure 26. Equivalent elastic strain for device A (F3=4000N)	Figure 28. Equivalent (von-Mises) Stress for device A (F3=4000N)
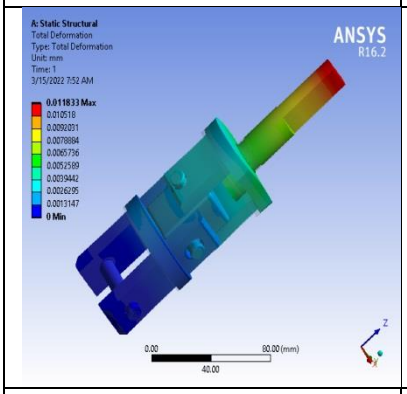	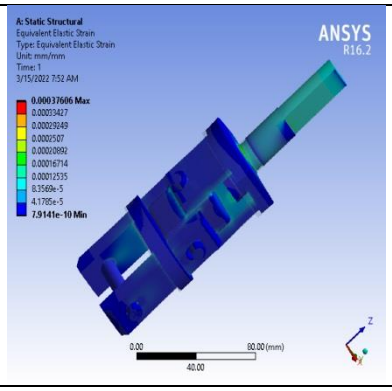	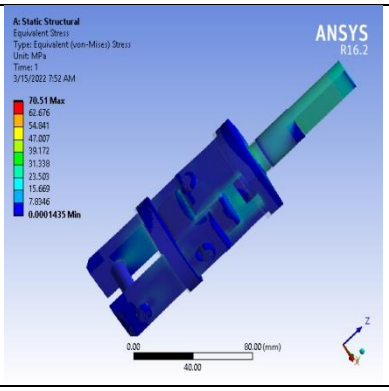
Figure 25. Total deformation for device B (F3=4000N)	Figure 27. Equivalent elastic strain for device B (F3=4000N)	Figure 29. Equivalent (von-Mises) Stress for device B (F3=4000N)
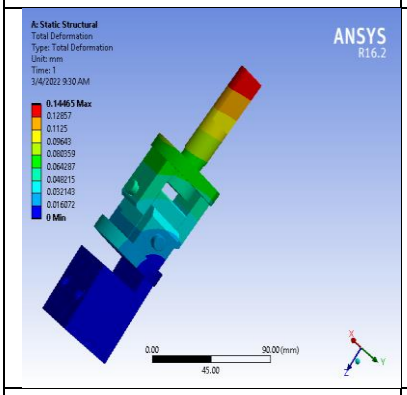	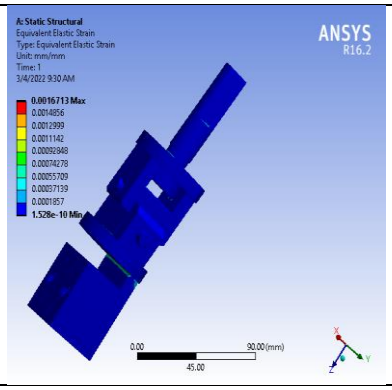	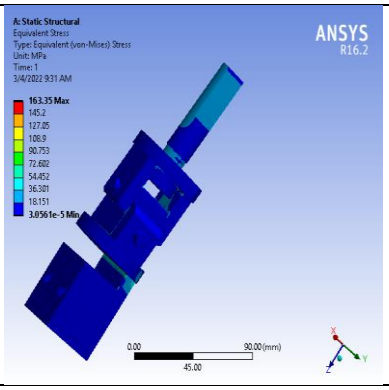
Figure 30. Total deformation for device A (F4=5000N)	Figure 32. Equivalent elastic strain for device A (F4=5000N)	Figure 34. Equivalent (von-Mises) Stress for device A (F4=5000N)

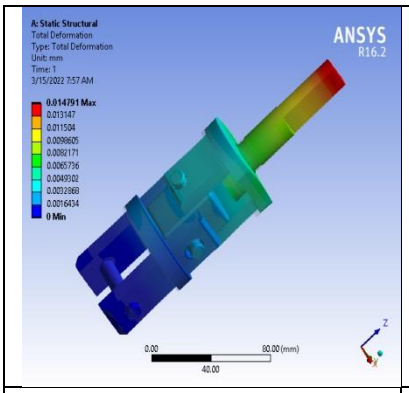

Figure 31. Total deformation for device B (F4=5000N)

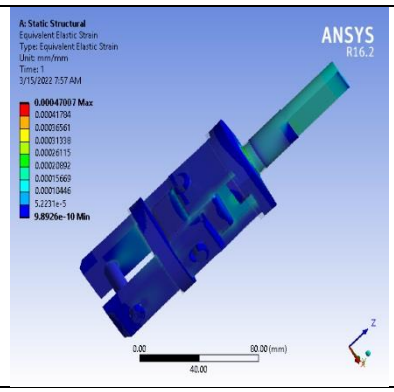

Figure 33. Equivalent elastic strain for device B (F4=5000N)

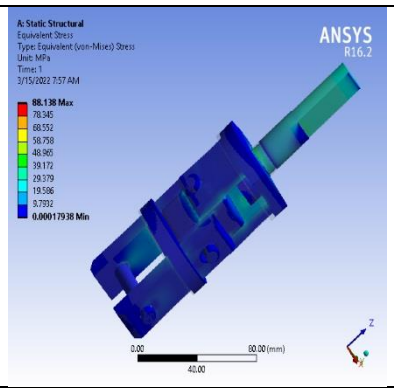

Figure 35. Equivalent (von-Mises) Stress for device B (F4=5000N)

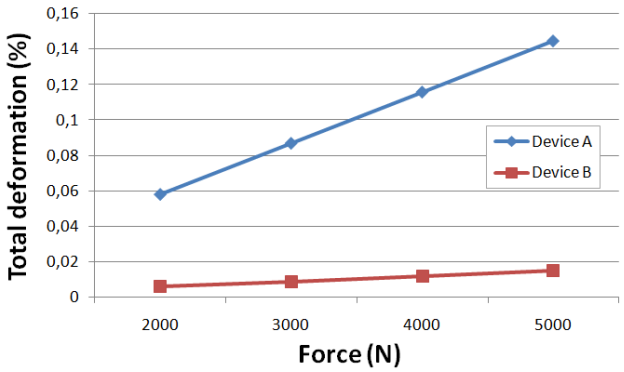

Figure 36. Representation of total deformation of devices A and B as a function of the forces exerted by the traction machine

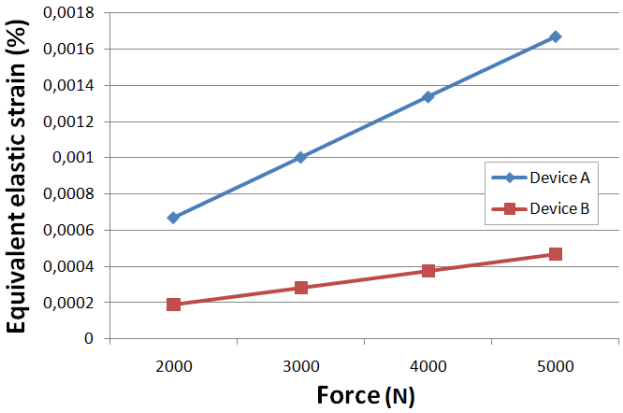

Figure 37. Representation of equivalent elastic strain of devices A and B as a function of the forces exerted by the traction machine

Device A:

Figures (12, 18, 24 and 30) show the values of the total deformation for each point of the device A. We notice that the maximum value recorded is (0.14465%) at the point of application of the force F =5000N. On the other hand, the value recorded at the application of the force (2000N) is (0.057858%). We can conclude that the deformation varies proportionally to the force. It is also noteworthy that the deformation becomes zero at point B (fixed point).

Figures (14, 20, 26, and 32) show the values of the equivalent elastic deformation for each point of device A. We notice that the maximum value recorded is (0.016713 at the point of application of the force 5000N. Furthermore, the value recorded at the application of the force (2000N) is (0.0006685). It is also worth mentioning that the minimum value of the equivalent elastic deformation is (1.528e-10) related to the force (5000N) and (6.1121e-11) at the application of the force (2000N).

Figures (16, 22, 28, and 34) show the equivalent Von-Mises stresses that define the elasticity for device A. It brought to our attention that the maximum value recorded is (163.35 from the force F=5000N. At the application of the force (2000N), the recorded value is (65.342). This maximum value is displayed at the most stressed points of the device.

On the other hand, the minimum value of the equivalent elastic deformation is (1.528e-10) related to the force (5000N) and (6.1121e-11) when applying a 2000N force.

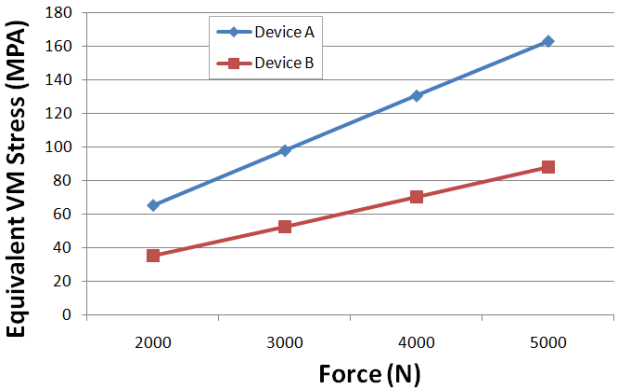

Figure 38. Representation of equivalent (Von Mises) stress of devices A and B as a function of the forces exerted by the traction machine

Device B:

Figures (13, 19, 25 and 31) show the values of the total deformation for each point of the device B. We note that

the maximum value recorded is (0.014791%). This deformation is recorded at the point of application of the force F=5000N. When applying the force (200N), the value recorded is (0.005916%). The total deformation value becomes zero at the fixed-point A of the device.

Figures (15, 21, 27 and 33) show the values of the equivalent elastic deformation for each point of device B. We note that the maximum value recorded is (0.00047007) at the point of application of the force F=5000N. Moreover, when applying the force (2000N), the value recorded is (0.00018803). We should mention that the minimum value of the equivalent elastic deformation is (9.8926e-10) related to the force (5000N) and (3.9571e-10) at the application of the force (2000N).

Figures (17, 23, 29 and 35) show the equivalent Von-Mises stresses that define the elasticity for device B. We note that the maximum value recorded is (88.138) when applying the force F=5000N, and (35.255) when applying the force F=2000N. This maximum value is displayed at the most stressed points of the device.

On the other hand, the minimum value of the equivalent elastic deformation is (0.00017938) for (5000N) and (7.1752e-5) for (2000N) at point A (point of force application).

According to the graphical presentations in figures (36, 37 and 38), we see that the different values of total strain, equivalent Von-Mises stress and equivalent elastic strain vary proportionally with the studied forces.

4. Conclusion

The realization of the docking and alignment device facilitated the fixation of the transversally cut specimens, and of the CT and DCB types to the jaws of the traction (or fatigue) machines. The CATIA V5 software was used to design these devices.

The stresses applied on these devices were simulated by the ANSYS software, in order to know their mechanical behavior. For this purpose, the different criteria obtained during the simulation are: the total deformation, the equivalent elastic deformation and the equivalent Von Mises stress.

The results obtained for device A show that the total strain has a maximum value of 0.14465%, the maximum value of the equivalent elastic strain is 0.016713mm/mm and the equivalent Von Mises stress is 163.35 MPa.

The results obtained with device B show that the total strain has a maximum value of 0.014791%, the maximum value of the equivalent elastic strain is 0.00047007mm/mm and the equivalent Von Mises stress is 88.138 MPa.

Based on these results, we can conclude that the device will be able to withstand the various tests performed by the tensile machine since they do not exceed the value of the elastic limit of the material.

References

[1] Languedoc-Roussillon. Guide d'aide au choix des matériaux des réseaux d'eau potable et/ou d'assainissement. Charte Qualité des réseaux d'eau potable et d'assainissement. Swelia (2015) pp 19-27.

[2] Montes J. C. Impacts des stratégies d'exploitation de réseaux intérieurs sur la durabilité de canalisations d'eau chaude. Laboratoire d'Etudes des Matériaux en Milieux Agressifs. Université de La Rochelle. (2011) pp 99-102.

[3] Guidara M.-A. Analyse des conditions de rupture des conduites d'adduction d'eau potable en polyéthylène, sous l'effet d'écoulement transitoire, en présence d'un défaut. Mécanique et Energétique, Université de Lorraine Et École Nationale d'Ingénieurs de Sfax. (2016) pp.100-109

[4] Hadi H.-J. Evaluation the effect of residual stress on fracture of polyethylene pipe under pressure loading. Basrah Journal for Engineering Sciences (2016). 16(2) pp. 71-78.

[5] Kukreja N. Design and implementation of soil drilling machine using NX 12 and CATIA V5 fabrication techniques. Materials Today: Proceedings (2021). https://doi.org/10.1016/j.matpr.2021.04.384

[6] Mouallif, I., Chouaf, A., El Amri, A., Benali, A. (2011) Effects of alumino-thermic welding defects on the rails mechanical behaviour. Mecanique & Industries, 12(5) (2011) pp. 343–351. DOI: 10.1051/meca/2011119

[7] Nachippan N.-M., Alphonse M., Raja V.K.B., Palanikumar K., Kiran R.S.U., Krishna V. Numerical analysis of natural fiber reinforced composite bumper. Materials Today: Proceedings (2021). https://doi.org/10.1016/j.matpr.2021.02.045

[8] Lasfar, S., Mouallif, I., Latrach, A., Choukir, A., Diab, A. Resistance of two different types of concrete pipes used in sewer systems under sulfuric acid and sodium sulfate attacks. Journal of Materials and Environmental Science (2015), 6(11) pp. 3002–3014.

[9] Mouallif, I., Latrach, A., Chergui, M., Hangouët, J.-P., Barbe, N. Degradation of dynamic mechanical properties of glass fiber reinforced polyester composite pipes after immersion in various temperatures. Journal of Composite Materials (2014), 48(24), pp. 3025–3034. https://doi.org/10.1177/0021998313504605.

[10] Mouallif, I., Mouallif, Z., Benali, A., Sidki, F. Finite element modeling of the aluminothermic welding with internal defects and experimental analysis. MATEC Web of Conferences (2012), 100002.https://doi.org/10.1051/matecconf/20120100002.

[11] L. Laiarinandrasana, E. Gaudichet, S. Oberti, C. Devilliers. Effects of aging on the creep behaviour and residual lifetime assessment of polyvinyl chloride (PVC) pipes. International Journal of Pressure Vessels and Piping. (2011) doi:10.1016/j.ijpvp.2011.01.002

[12] Hong Zhang, Keita Fujiki, Kazumi Ido, Natsumi Kusayanagi, Daiki Sakagami, Junjie Li, Yosuke Okamura. Tensile testing of freestanding polymer thin films with non-standard geometries. Polymer Testing. (2020) https://doi.org/10.1016/j.polymertesting.2020.106825

[13] Say A. Malak. Tensile stress strain model of polyvinyl chloride/calcium carbonate (PVC/CaCO3) nanocomposite plank. Results in materials. (2021) https://doi.org/10.1016/j.rinma.2021.100193

[14] Ahmed Fauzan Zakki. Aulia Windyandari. Simplified FE Model and experimental study on the tensile properties of the glass fiber reinforced polyester polymer. Heliyon. (2022) https://doi.org/10.1016/j.heliyon.2022.e10999

[15] Shiv Kumar Ji Yadav, Ajitanshu Vedrtnam, Dheeraj Gunwant. Experimental and numerical study on mechanical behavior and resistance ton natural weathering of sugarcane leave reinforced polymer composite. Construction and Building Materials. (2020). https://doi.org/10.1016/j.conbuildmat.2020.120785

[16] Alexandru Isaincu, Micota Dan, Viorel Ungureanu, Liviu Marşavina, Numerical investigation on the influence of fiber orientation mapping procedure to the mechanical response of short-fiber reinforced composites using Moldflow, Digimat and Ansys software, Materials Today: Proceedings, Volume 45, Part 5, 2021, Pages 4304-4309, ISSN 2214-7853, https://doi.org/10.1016/j.matpr.2020.12.792.

[17] F. Giorgetti, R. Lombroni, V.G. Belardi, G. Calabrò, M. Dalla Palma, P. Fanelli, M. Fulici, G. Ramogida, F. Vivio, Vertical displacement events analysis using MAXFEA code in combination with ANSYS APDL in the final design stage of the DTT vacuum vessel, Fusion Engineering and Design, Volume 184, 2022, 113273, ISSN 0920-3796, https://doi.org/10.1016/j.fusengdes.2022.113273.

[18] Eneyw Gardie, Velmurugan Paramasivam, Habtamu Dubale, Ewnetu Tefera Chekol, Senthil Kumaran Selvaraj, Numerical analysis of reinforced carbon fiber composite material for lightweight automotive wheel application, Materials Today: Proceedings, Volume 46, Part 17, 2021, Pages 7369-7374, ISSN 2214-7853, https://doi.org/10.1016/j.matpr.2020.12.1047.

[19] K.S. Ashraff Ali, D. Joseph Manuel, M. Balamurugan, M. Sangili Murugan, Analysis of composite leaf spring using ANSYS software, Materials Today: Proceedings, Volume 37, Part 2, 2021, Pages 2346-2351, ISSN 2214-7853, https://doi.org/10.1016/j.matpr.2020.08.068.